THE PROTEIN SOCIETY

# Calorimetric and spectroscopic investigation of the interaction between the C-terminal domain of Enzyme I and its ligands

**Young-Joo Yun and Jeong-Yong Suh***

Department of Agricultural Biotechnology, WCU Biomodulation major, Seoul National University, 599 Gwanak-ro, Gwanak-gu, Seoul 151-921, Korea

Received 18 June 2012; Revised 24 August 2012; Accepted 26 August 2012
DOI: 10.1002/pro.2152
Published online 30 August 2012 proteinscience.org

**Abstract: Enzyme I initiates a series of phosphotransfer reactions during sugar uptake in the bacterial phosphotransferase system. Here, we have isolated a stable recombinant C-terminal domain of Enzyme I (EIC) of *Escherichia coli* and characterized its interaction with the N-terminal domain of Enzyme I (EIN) and also with various ligands. EIC can phosphorylate EIN, but their binding is transient regardless of the presence of phosphoenolpyruvate (PEP). Circular dichroism and NMR indicate that ligand binding to EIC induces changes near aromatic groups but not in the secondary structure of EIC. Binding of PEP to EIC is an endothermic reaction with the equilibrium dissociation constant ($K_D$) of 0.28 m*M*, whereas binding of the inhibitor oxalate is an exothermic reaction with $K_D$ of 0.66 m*M* from calorimetry. The binding thermodynamics of EIC and PEP compared to that of Enzyme I (EI) and PEP reveals that domain–domain motion in EI can contribute as large as ~−3.2 kcal/mol toward PEP binding.**

**Keywords: phosphotransferase system; protein–ligand interaction; binding thermodynamics; domain–domain interaction**

## Introduction

Enzyme I (EI) is a ~130-kDa dimeric protein (575 aa) that initiates a cascade of phosphotransfer reactions in the bacterial phosphotransferase system.[1–3] EI catalyzes two reversible reactions: an $Mg^{2+}$-dependent autophosphorylation reaction using phosphoenolpyruvate (PEP) as a substrate, and a phosphotransfer reaction to histidine-containing phosphocarrier protein, HPr. EI comprises a stable N-terminal domain (EIN) which has a catalytic αβ domain and an HPr-binding α domain, and a PEP-binding C-terminal domain (EIC).[4] First, EIC binds to PEP and phosphorylates the active site His189 in the αβ domain of EIN, and then the phosphoryl group is transferred to HPr bound on the α domain of EIN. EIN is a highly stable protein and the structure has early been determined by X-ray crystallography and NMR spectroscopy.[5,6] On the other hand, EIC is prone to proteolysis, which made it difficult to isolate recombinant EIC protein for biochemical and biophysical characterization.[7] EIC is responsible for the dimerization of EI, whereas EIN exists

*Abbreviations:* EI, Enzyme I; EIC, C-terminal domain of Enzyme I; EIN, N-terminal domain of Enzyme I; HPr, histidine-containing phosphocarrier protein; HSQC, heteronuclear single quantum coherence; PEP, phosphoenolpyruvate; PTS, phosphotransferase system.

Additional Supporting Information may be found in the online version of this article.

Grant sponsor: WCU (World Class University) program; Grant number: R31-10056; Grant sponsor: National Research Foundation of Korea (NRF) grant funded by the Ministry of Education, Science and Technology; Grant number: 2011-0025901, 2010-0025883.

*Correspondence to: Jeong-Yong Suh, WCU Biomodulation major, Department of Agricultural Biotechnology, Seoul National University,599 Gwanak-ro, Gwanak-gu, Seoul 151-921, Korea. E-mail: jysuh@snu.ac.kr

exclusively as a monomer. Crystal structures of EI have suggested the presence of multiple conformational states during the enzyme reactions, but it is not clear how the domain motions evolve with the substrate binding and phosphotransfer reactions.[8–10] Characterizing the interaction of isolated EIC with its ligands and also with EIN would provide useful information to understand the mechanism underlying the domain motions.

There have been efforts for isolation and biophysical characterization of recombinant EIC. Erni group determined the first crystal structure of EIC of a thermophilic bacterium, *Thermo tengcongensis*,[11] and then Roseman group successfully isolated EIC of *Escherichia coli* using an intein system and characterized its interaction with the ligands by spectroscopic and kinetic analysis.[12] Isolation of EIC of *E. coli*, however, still suffered from proteolysis during expression, and protein ligation was the only method of choice.[12] Here we have expressed multiple constructs of EIC of *E. coli* varying the linker region between EIN and EIC, and obtained a construct that expresses stable EIC in an intact form. We have characterized the interaction of EIC with its substrates and inhibitor, and also with EIN using calorimetry, circular dichroism (CD), and NMR spectroscopy.

## Results and Discussion

We designed three EIC constructs varying the linker region between EIN and EIC into a pET11a vector and examined the expression of the recombinant proteins. The linker region forms a long helix from residue Thr232 to residue Lys257, followed by a short β bridge (Ala261-Val269) that connects the linker helix to the $(\alpha\beta)_8$ barrel fold of EIC. The $EIC_{231–575}$ construct contains the linker helix followed by EIC, whereas the $EIC_{260–575}$ construct lacks the whole linker helix. Finally, the $EIC_{270–575}$ construct contains only the $(\alpha\beta)_8$ barrel fold of EIC with both the linker helix and the β bridge removed. Figure 1(A) shows the three-dimensional structure of EI in a ribbon diagram, where EIN is colored in gray, EIC in blue, and the linker helix and the β bridge in red. Only one subunit of the EI dimer is shown for visual clarity, and the N-terminal residues of individual EIC constructs in this study are shown as a space-filling model in orange. When the constructs were transformed into an *E. coli* strain BL21star(DE3) and overexpressed in Luria Broth media, $EIC_{231–575}$ and $EIC_{270–575}$ appeared as single bands in the sodium dodecyl sulfate-polyacrylamide gel electrophoresis (SDS-PAGE) [Fig. 1(B)]. $EIC_{260–575}$ exhibited a lower expression level and an additional band with a slightly lower molecular weight could be observed implying a proteolytic cleavage. We then checked whether the expressed proteins

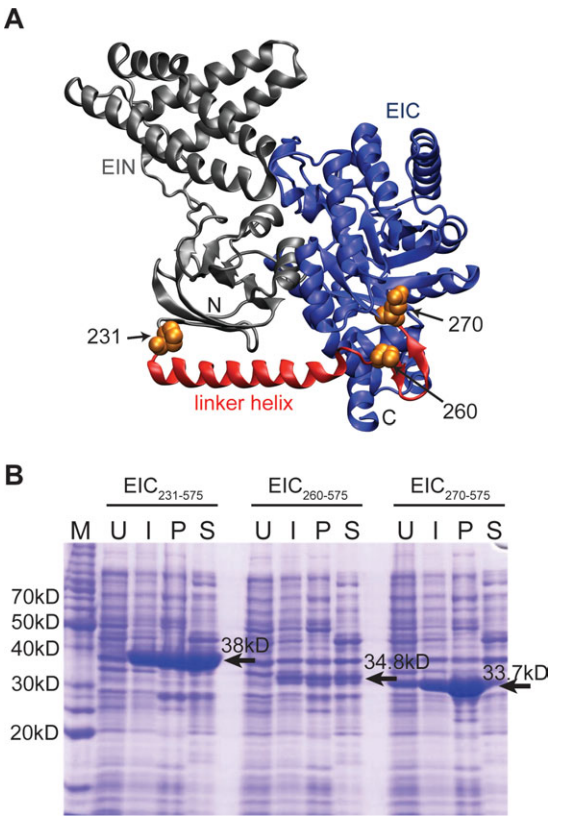


**Figure 1.** (A) The three-dimensional crystal structure of EI of *Escherichia coli* (from Protein Data Bank code 2HWG) as a cartoon diagram. EIN is colored in gray, EIC in blue, and the linker helix between EIN and EIC in red. The N-terminal residues (Pro231, Pro260, and Glu270) of the recombinant EIC constructs used in this study are shown as space-filling models in orange color. (B) Overexpression and solubility of recombinant $EIC_{231–575}$, $EIC_{260–575}$, and $EIC_{270–575}$ from SDS-PAGE. Arrows and expected molecular weights of individual proteins are drawn to indicate the bands from overexpressed proteins. Lanes: M (size marker), U (uninduced cell), I (induced cell using IPTG), P (pellet), S (supernatant). Samples for P and S are obtained by centrifugation after cell lysis. [Color figure can be viewed in the online issue, which is available at wileyonlinelibrary.com.]

formed a soluble fold or an inclusion body. $EIC_{270–575}$ mostly formed an inclusion body likely due to misfolding, whereas $EIC_{231–575}$ largely remained as a soluble form [Fig. 1(B)]. The absence of proteolysis of $EIC_{270–575}$ is possibly due to its formation of an inclusion body before proteolysis took place during the overexpression. Our result is consistent with previous studies,[12,13] and indicates that keeping the linker helix is critical to confer proteolytic stability on EIC, while the short β bridge is important for proper folding of EIC. $EIC_{231–575}$ was stable during the purification using chromatography at a room temperature, and used for all experimental measurements hereafter.

EIN can switch between two conformational states which differ in their domain–domain orientation of the α and αβ domains. The first

conformational state is optimal for the phosphotransfer reaction between EIN and HPr, and the second conformational state is relevant for the autophosphorylation reaction between EIN and EIC.[8–10] Isolated EIN adopts predominantly the first conformational state in solution, but the interaction with EIC requires a switch to the second conformational state.[5] Exchange between the two conformational states entails a large domain–domain motion between α and αβ domains within EIN, which would cause chemical shift perturbation at the interface between the domains. In light of this, we monitored spectral changes in the $^{1}H-^{15}N$ correlation spectra of EIN titrating with EIC to investigate their interactions.

We titrated 0.2 m*M* of $^{2}H,^{15}N$-EIN with up to 0.8 m*M* of $EIC_{231–575}$, but could not observe significant chemical shift changes or line broadening. The lack of chemical shift perturbation and line-broadening implies that the intrinsic binding between separate EIN and EIC would be extremely weak [black and green cross-peaks in Fig. 2(A)]. Weak affinity between covalently-linked domains has been observed in other phosphotransferase system (PTS) proteins when the connecting linker is removed.[14] Domains of weak affinity easily achieve fast dissociation kinetics, but require high local concentrations for fast association. A covalent linker connecting the domains makes the association a unimolecular reaction which assures fast association kinetics defined by the size of the linker.[15] This can be a useful strategy for PTS in which rapid association and dissociation coupled with phosphotransfer reactions are important for prompt sugar uptake and phosphorylation in bacteria.

We examined the functional complementarity between EIC and EIN for the phosphotransfer reaction. It has been reported that EIC can phosphorylate EIN from a biochemical assay using $^{32}P$-PEP as a substrate.[12,16] When we added PEP to the mixture of EIN and $EIC_{231–575}$ after titration, we could immediately observe the chemical shift changes due to the phosphorylation reaction of EIN [red cross-peaks in Fig. 2(A)]. Characteristic chemical shift changes could be observed for Gly10, Gly178, Gly185, and Gly204 among others, and these cross-peaks returned to their original position when EIN was dephosphorylated. The residues with chemical shift perturbation are drawn as space-filling models on the three-dimensional structure of EIN to visualize their spatial distribution [Fig. 2(B)]. The chemical shift changes were consistent with the phosphorylated EIN [blue cross-peaks in Fig. 2(A)], which was obtained using EIN mixed with HPr, EI, and PEP, where the phosphoryl group was transferred from EI to HPr and finally to EIN.[17,18] Our result shows that separate EIN and EIC formed a functional complex for the phosphotransfer reaction *in vitro* and

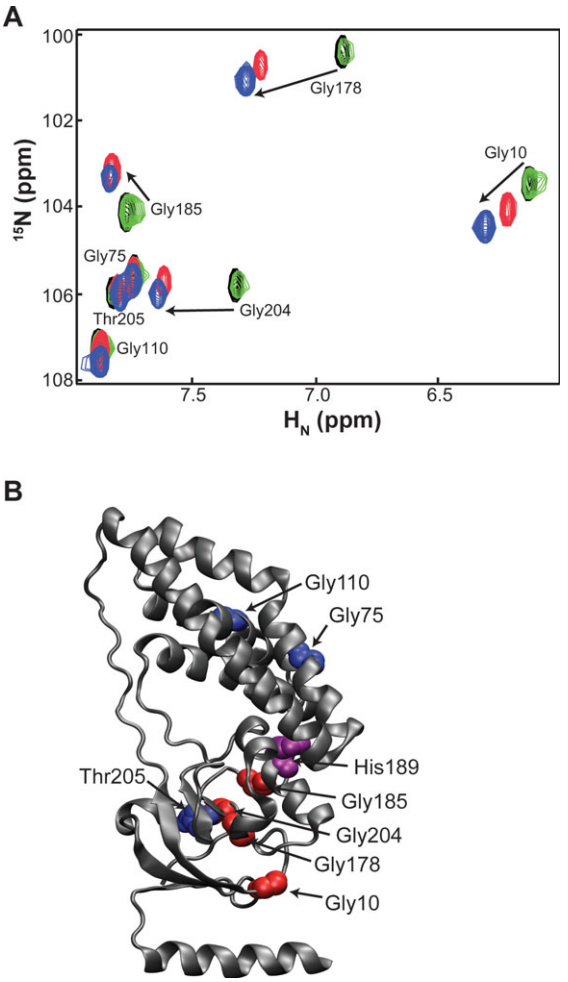


**Figure 2.** (A) Chemical shift changes of EIN in the selected regions of $^{1}H-^{15}N$ HSQC spectra: 0.2 m*M* $^{2}H,^{15}N$-EIN (black), 0.2 m*M* $^{2}H,^{15}N$-EIN with 0.8 m*M* unlabeled EIC (green), 0.2 m*M* $^{2}H,^{15}N$-EIN with 0.8 m*M* EIC and 10 m*M* PEP (red), and 0.2 m*M* of phosphorylated $^{15}N$-EIN by 2 μ*M* EI, 2 μ*M* HPr, and 10 m*M* PEP (blue). Assignments are shown for the cross-peaks of unphosphorylated EIN, and chemical shift changes upon phosphorylation are indicated by arrows. (B) The residues that appear in the HSQC spectra are mapped on the three-dimensional structure of EIN (from Protein Data Bank code 3EZA) as space-filling models, where the residues with chemical shift perturbation by phosphorylation are colored in red and those without chemical shift perturbation are colored in blue. Active site His189 is shown in purple as a space-filling model. [Color figure can be viewed in the online issue, which is available at wileyonlinelibrary.com.]

the two domains would readily dissociate after the phosphotransfer reaction. There was no line-broadening in the heteronuclear single quantum coherence (HSQC) spectra of $^{15}N$-EIN with EIC, regardless of the presence of PEP, implying that the dynamics of EIN little changed by EIC and ligands in the experimental condition. We exclude the possibility that contaminating EI and HPr in the preparation of EIC or EIN have caused the phosphorylation reaction in our study. First, EIN was not

**Table I.** *Equilibrium Dissociation Constants ($K_D$), Binding Enthalpies ($\Delta H$), and Entropies ($\Delta S$) Obtained from Least-Squares Fitting of One Set of Sites Binding Model to the Experimental ITC Data for the Interaction Between EIC and Its Ligands at pH 7.4 Under Different Buffer Conditions*

| Ligands | Buffer (pH 7.4) | $K_D$ (m*M*) | $\Delta H$ (kcal/mol) | $\Delta S$ (cal/mol/K) |
|---|---|---|---|---|
| PEP | Tris | 0.28 ± 0.14 | 1.76 ± 0.98 | 22.2 |
| PEP | HEPES | 0.24 ± 0.08 | 0.99 ± 0.15 | 19.9 |
| PEP | Phosphate | 0.17 ± 0.05 | 0.54 ± 0.08 | 19.1 |
| Oxalate | Tris | 0.66 ± 0.24 | -0.63 ± 0.26 | 12.4 |
| Oxalate | HEPES | 0.42 ± 0.05 | -0.94 ± 0.12 | 12.3 |
| Oxalate | Phosphate | 0.44 ± 0.14 | -0.62 ± 0.20 | 13.3 |

phosphorylated when we added PEP to EIN without EIC, so the preparation of EIN was free of contaminating EI and HPr. Second, we monitored the phosphorylation of the A domain of the mannitol transporter, Enzyme $II^{Mtl}$ ($IIA^{Mtl}$), which could be phosphorylated by EI and HPr. If contaminating EI and HPr in the preparation of EIC caused the phosphorylation of EIN, they would also phosphorylate $IIA^{Mtl}$ in the same manner. Phosphorylation of $^{15}$N-$IIA^{Mtl}$ can be immediately identified by the chemical shift changes in the $^{1}H-^{15}N$ correlation spectrum. When we incubated $^{15}$N-$IIA^{Mtl}$ with EIC using the same buffer composition as was used to phosphorylate EIN, the spectra clearly indicated that $IIA^{Mtl}$ remained in the unphosphorylated state (Supporting Information Fig. 1S). Taken together, the phosphorylation of EIN resulted from the direct interaction between EIN and EIC, rather than from contaminating EI and HPr. We note that $EIN_{1–249}$ and $EIC_{231–575}$ share part of the linker helix between 231 and 249. As the two domains could form a functional complex for the phosphotransfer reaction, precise orientation of the linker helix may not be critical in the reaction complex between EIN and EIC.

We also examined whether the transient complex between EIN and EIC could be captured when PEP was bound to EIC. As EIN released from EIC after the phosphorylation reaction, we used EIN(H189Q) mutant where the active site His189 was replaced by a isosteric glutamine residue that could not be phosphorylated. The NMR spectra of 0.2 m*M* $^{15}$N-EIN(H189Q) mixed with 0.8 m*M* $EIC_{231–575}$, 4 m*M* $MgCl_2$, and 10 m*M* PEP did not show noticeable chemical shift changes (data not shown). Using the equilibrium dissociation constant ($K_D$ ~0.28 m*M*) of EIC and PEP from isothermal titration calorimetry (ITC) study in Table I (see below), more than 95% of EIC is bound to PEP in this concentration. We infer that the conformational state of EIN that binds to EIC is thermodynamically unstable, so that the phosphotransfer reaction complex between EIN and EIC represents a metastable transient state.

Far UV CD spectroscopy (200–250 nm) provides information on the content of secondary structures, and near UV CD spectroscopy (250–350 nm) provides information on the tertiary structures from asymmetric environments of aromatic chromophores. The far UV CD spectrum of $EIC_{231–575}$ showed the presence of significant secondary structures, where two minima at 208 and 222 nm were characteristic signatures of an α-helix [Fig. 3(A)]. When we added the substrates, PEP and pyruvate, or the inhibitor oxalate to $EIC_{231–575}$, we could not observe significant changes in the far UV CD spectra of $EIC_{231–575}$, indicating that ligand binding did not largely affect the secondary structures of EIC [Fig. 3(A)]. On the other hand, the near UV CD spectra of $EIC_{231–575}$ exhibited noticeable differences between the free and the ligand-bound states between 260 and 290 nm [Fig. 3(B)]. As the near UV CD spectra imply that ligand binding affected aromatic residues, we examined the 1D $^{1}$H-NMR spectra of $EIC_{231–575}$ in the aromatic region upon ligand binding. To remove amide proton signals $EIC_{231–575}$ and its complex with ligands were prepared in the same buffer using $D_2O$. The $^{1}$H-NMR spectra of $EIC_{231–575}$ revealed manifest chemical shift changes in the aromatic region, where the changes were more pronounced in the binding to PEP or oxalate than the binding to pyruvate [Fig. 3(C)]. $^{1}$H-NMR spectra of methyl region of $EIC_{231–575}$ showed modest chemical shift changes upon ligand binding [Fig. 3(D)]. $EIC_{231–575}$ has 2 tryptophan, 6 tyrosine, 13 thirteen phenylalanine residues, and none of the aromatic residues are within 6 Å from the bound oxalate in the crystal structure (PDB code: 2HWG). However, the crystal structure of EIC from *Thermoanaerobacter tengcongensis* recently showed a conformational change of Phe354 upon binding to PEP.[19] As Phe354 is conserved in EIC of *E. coli*, it likely contributed to the change in the CD and NMR spectra in this study. In addition, Tyr459 and Tyr474 are the nearest neighboring aromatic residues to the PEP binding site, which may have contributed to the spectroscopic changes observed in this study.

We measured the equilibrium binding between $EIC_{231–575}$ and its ligands at 25°C using ITC. It is known that the dimeric form of EI is the active form and the monomer–dimer equilibrium can vary with experimental conditions.[12,20,21] Previously, the $K_D$ for the dimerization of $EIC_{256–575}$ in the presence of 5 m*M* $MgCl_2$ and 100 m*M* NaCl at pH 7.5 and 25°C was reported as ~6 n*M* from analytical ultracentrifugation.[12] When we loaded a serial dilution of

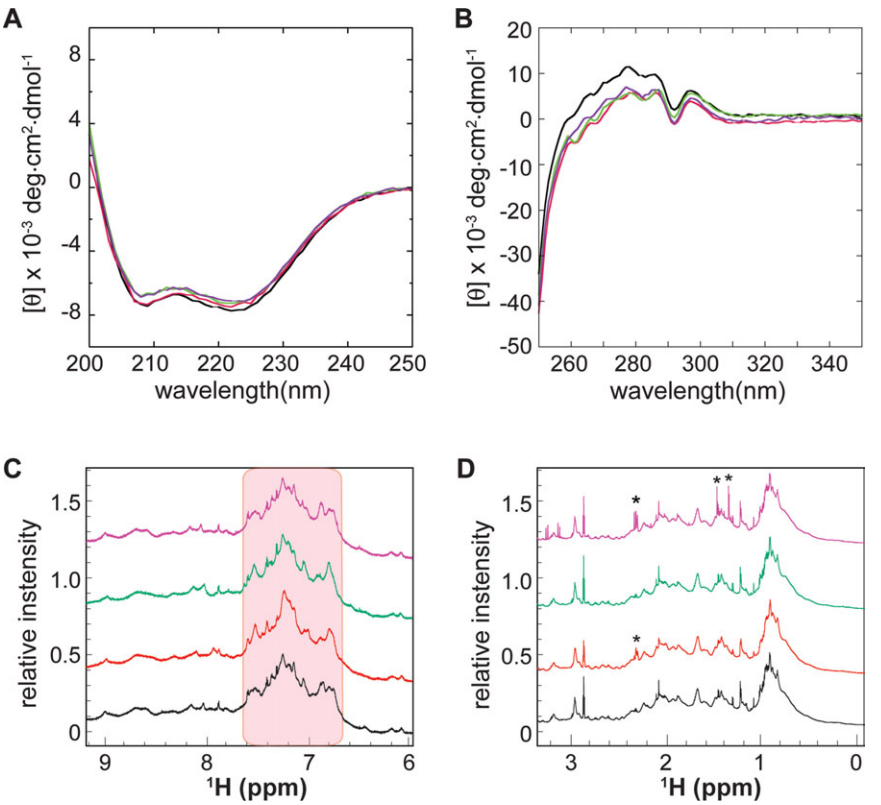


**Figure 3.** Circular dichroism and 1D $^1$H-NMR spectra of $EIC_{231–575}$ (black) and $EIC_{231–575}$ with PEP (red), oxalate (green), and pyruvate (purple) at 25°C. Circular dichroism spectra were presented as (A) mean residue ellipticity at far UV wavelength of 200–250 nm, and (B) molar ellipticity at near UV wavelength of 250–350 nm. (C) 1D $^1$H-NMR spectra of aromatic proton region obtained using a Bruker 600 MHz NMR spectrometer. The chemical shift changes of the aromatic proton region are highlighted in pink. (D) 1D $^1$H-NMR spectra of methyl proton region, where the asterisks (*) denote signals from contaminating chemicals. [Color figure can be viewed in the online issue, which is available at wileyonlinelibrary.com.]

$EIC_{231–575}$ from 200 μ*M* to 2 μ*M* onto the Superdex 200 size exclusion column, the elution volume was constant, indicating that $EIC_{231–575}$ was a dimer in the given concentration range. If we assume that >90% of 2 μ*M* $EIC_{231–575}$ is dimeric based on the size exclusion chromatography, we can calculate the upper limit of $K_D$ as ~10 n*M*. We also carried out the size exclusion chromatography of EIC with ligands, and the elution volume did not change, hence the ligand-bound EIC was also a dimer. In the current ITC measurement, we used 0.25–0.5 m*M* of EIC in the cell and titrated with 3–10 m*M* of ligands. At this concentration range, more than 80% of EIC is predicted to be dimeric during the titration. The measured $K_D$ between $EIC_{231–575}$ and PEP was 0.28 m*M*, which was close to the $K_D$ values (0.22–0.28 m*M*) obtained from previous spectroscopic studies [Fig. 4(A)].[12] The $K_D$ between $EIC_{231–575}$ and oxalate was 0.66 m*M*, so the binding was 2.4 times weaker than the binding to PEP [Fig. 4(B)]. The stoichiometry of the binding of $EIC_{231–575}$ to the ligands indicated that each monomeric subunit of the EIC dimer bound to one molecule of the ligand with a comparable affinity.

We note that the apparent binding enthalpy ($\Delta H_{binding}$) measured by ITC is the sum of the intrinsic reaction enthalpy ($\Delta H_{react}$; independent of the buffer) and the ionization enthalpy ($\Delta H_{ionization}$) from the buffer, as was described by Freire and coworker.[22] $\Delta H_{react}$ can be obtained by performing ITC in buffers with different ionization enthalpies. We carried out titration experiments at pH 7.4 using sodium phosphate and 4-(2-hydroxyethyl)-1-piperazineethanesulfonic acid (HEPES) buffers as well as Tris-HCl buffer, which exhibited a wide range of the ionization enthalpies at 25°C (0.98 kcal/mol, 5.03 kcal/mol, and 11.16 kcal/mol for phosphate, HEPES, and Tris-HCl buffer, respectively).[23] When $\Delta H_{binding}$ is plotted as a function of $\Delta H_{ionization}$, the slope of the linear regression gives the number of protons released by the buffer (taken by the protein) upon binding and the *y*-intercept is $\Delta H_{react}$.[22] From the linear regression, the $\Delta H_{react}$ of $EIC_{231–575}$ for binding to PEP was 0.41 kcal/mol, and the $\Delta H_{react}$ for binding to oxalate was −0.75 kcal/mol [Fig. 4(C,D)]. Also, the slope of the linear regression indicated that ligand binding of $EIC_{231–575}$ involved little changes in the ionization states at the binding site. It is notable that the interaction between $EIC_{231–575}$ and PEP was an endothermic reaction, while the interaction between $EIC_{231–575}$ and the inhibitor oxalate was an exothermic reaction (Table I). Binding to

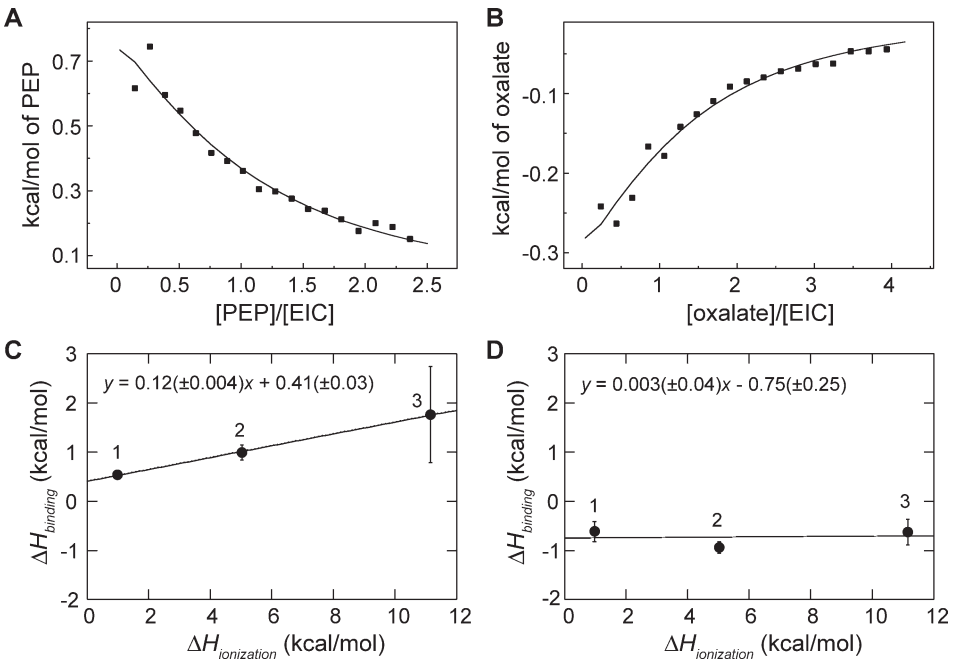


**Figure 4.** Integrated heats of injections from the titration between (A) PEP and EIC and (B) oxalate and EIC in 20 m*M* Tris-HCl buffer, pH 7.4, 100 m*M* NaCl, 2 m*M* β-mercaptoethanol, and 4 m*M* $MgCl_2$. The squares are the experimental data, and the lines represent the least-squares best-fit curves derived for one-set of sites binding model. The equilibrium dissociation constants and thermodynamic parameters are given in Table I. Enthalpy changes of binding ($\Delta H_{binding}$) as a function of the ionization enthalpy ($\Delta H_{ionization}$) of the reaction buffer for (C) PEP/EIC titration and (D) oxalate/EIC titration; 1, 20 m*M* sodium phosphate; 2, HEPES; 3, Tris-HCl, pH 7.4.The equations from the linear least-squares fits of the data are inserted in the figure.

PEP was driven by a favorable entropic contribution, so that hydrophobic interaction was important in the binding between EIC and PEP. On the other hand, binding to oxalate was driven by both enthalpic and entropic contributions, so that electrostatic interaction was important in the binding between EIC and oxalate. We also carried out the titration between $EIC_{231–575}$ and pyruvate, but could not observe a reliable binding isotherm due to small measured heat and weak binding. The weak binding between EIC and pyruvate was not unexpected as the Michaelis constant ($K_m$) for EI and pyruvate was reported to be ~2 m*M*, which was 10 times larger than the $K_m$ for EI and PEP.[24]

Previous ITC study reported that the $K_D$ between the active-site mutant EI(H189A) and PEP was ~1 μ*M*, so that the binding between EI and PEP was about two orders of magnitude stronger than the binding between $EIC_{231–575}$ and PEP.[25] The binding between EI(H189A) and PEP was also an endothermic reaction, where the free energy of the binding ($\Delta G$) was −8.1 ± 0.1 kcal/mol, the binding enthalpy ($\Delta H$) was 3.9 kcal/mol, and the binding entropy ($\Delta S$)was 40.8 cal/mol/K in the phosphate buffer.[25] These thermodynamic parameters compare to $\Delta G$ of −4.9 ± 1.4 kcal/mol, $\Delta H$ of 0.54 kcal/mol, and $\Delta S$ of 19.1 cal/mol/K for $EIC_{231–575}$ and PEP in this study (Table I). The larger binding affinity between EI and PEP compared to that of EIC and PEP suggests the contribution of domain–domain motions in EI toward PEP binding, which may be as large as −3.2 ± 1.4 kcal/mol of $\Delta\Delta G$ ($\Delta\Delta G = \Delta G_{EI:PEP} - \Delta G_{EIC:PEP}$). The large negative $\Delta\Delta G$ mainly results from favorable contribution of binding entropy, suggesting that large hydrophobic interactions are involved in the domain–domain motions in EI upon binding to PEP. The domain motions that potentially contribute to the observed $\Delta\Delta G$ include the conformational switching within EIN that could expose buried interfaces between α and αβ domains, and also the interaction between the αβ domain of EIN and EIC.

It has been reported that oxalate can inhibit the autophosphorylation reaction of EI using PEP with the inhibition constant ($K_I$) of 0.02 m*M*.[26] The large difference between $K_I$ and $K_D$ of EIC and oxalate can be explained by the mechanism of inhibition. Oxalate inhibits the autophosphorylation reaction by forming a tight complex with phosphorylated EI, where the binding would be stabilized significantly by the association between EIN and EIC sandwiching the inhibitor oxalate.[9] Hence, the $K_D$ of EIC and oxalate in this study accounts for the intrinsic binding of the inhibitor when the domain–domain association does not take place.

In conclusion, we show that separate EIN and EIC domains form a functional reaction complex which is very weak regardless of the presence of ligands. The substrate PEP binds to EIC stronger than the inhibitor oxalate, and the two ligands

exhibit an opposite sign of binding enthalpy. Finally, comparison of PEP binding to EI and EIC suggests that apparent equilibrium binding between multi-domain proteins and ligands can be significantly affected by domain–domain motions.

## Materials and Methods

### *Cloning, expression, and purification of EIC and EIN*

$EIC_{231–575}$, $EIC_{260–575}$, and $EIC_{270–575}$ were cloned into a pET11a vector (Novagen) without tags, and the new constructs were verified by DNA sequencing. The plasmids were transformed into an *E. coli* strain BL21star(DE3), and then grown in Luria Bertini or minimal media with $^{13}C_6$-glucose and $^{15}NH_4Cl$ as the sole carbon and nitrogen sources in $D_2O$. The protein expression was induced with 1 m*M* isopropyl-β-D-thiogalactopyranoside at an $A_{600}$ of ~0.8, and harvested by centrifugation after 4 h of induction. The cell pellet was resuspended with 50 mL (per liter of culture) of 50 m*M* Tris, pH 8.0, 2 m*M* β-mercaptoethanol, 1 m*M* EDTA, 1 m*M* phenylmethylsulfonyl fluoride, and a protease inhibitor cocktail tablet (Sigma-Aldrich, S8820 SIGMAFAST). The suspension was lysed by three passages through Emulsiflex (Avestin, Canada) after homogenizing and centrifuged at 24,000*g* for 20 min at 4°C. The supernatant fraction was filtered and loaded onto a DEAE anion exchange column (20 mL; GE Healthcare) with a 400-mL gradient of 1*M* NaCl. The fractions containing EIC were purified by size exclusion on a Superdex 200 column (GE Healthcare) equilibrated with 20 m*M* Tris-HCl, pH 7.4, 200 m*M* NaCl, and 2 m*M* β-mercaptoethanol, and then on a monoQ anion exchange column (8 mL; GE Healthcare) with a 160-mL gradient of 1*M* NaCl.

EIN (residue 1–249) was cloned into a pET11a vector (Novagen) without tags, and the active site His189 of EIN was mutated to Gln using the QuickChange kit (Stratagene). The plasmids of wild-type EIN and EIN(H189Q) were individually transformed into an *E. coli* strain BL21star(DE3), and then grown in either Luria Bertini or minimal media with $^{15}NH_4Cl$ as the sole nitrogen source in $H_2O$ or $D_2O$. EIN proteins were expressed and purified as previously described.[17]

### *NMR spectroscopy of EIN with EIC*

NMR spectra were recorded at 30°C on a Bruker Avance 600 MHz or 900 MHz spectrometer equipped with an *x,y,z*-shielded gradient triple resonance probe. To examine EIN upon binding to EIC, 0.8 m*M* unlabeled $EIC_{231–575}$ was titrated into 0.2 m*M* $^2H,^{15}N$-labeled EIN with or without 10 m*M* PEP in 20 m*M* Tris-HCl, pH 7.4, 100 m*M* NaCl, 1 m*M* EDTA, 2 m*M* β-mercaptoethanol, and 4 m*M* $MgCl_2$. In addition, 0.2 m*M* $^{13}C,^{15}N$-labeled EIN(H189Q) and 0.8 m*M* unlabeled $EIC_{231–575}$ were used with or without 10 m*M* PEP in 20 m*M* Tris-HCl, pH 7.4, 100 m*M* NaCl, 1 m*M* EDTA, 2 m*M* β-mercaptoethanol, and 4 m*M* $MgCl_2$. Spectra were processed using the NMRPipe program and analyzed using the NMRView program.[27,28] For 1D $^1H$-NMR, 0.3 m*M* unlabeled $EIC_{231–575}$ were used with 5 m*M* of PEP, oxalate, and pyruvate in 20 m*M* Tris-HCl, pH 7.4, 100 m*M* NaCl, 1 m*M* EDTA, 2 m*M* β-mercaptoethanol, and 4 m*M* $MgCl_2$. The samples for 1D $^1H$-NMR were first prepared in $H_2O$-based buffer, lyophilized, and then dissolved in the same volume of $D_2O$.

### *Circular dichroism of EIC with PEP, oxalate, and pyruvate*

CD spectroscopy was conducted at 25°C using a with Chirascan™-plus CD spectrometer. Wave scans were acquired by sampling data at 1 nm intervals between 200 and 250 nm for far UV CD measurement and between 250 and 350 nm for near UV CD measurement. Far UV CD spectroscopy was carried out using 10 μ*M* of $EIC_{231–575}$ and 4 m*M* of substrates in 50 m*M* sodium phosphate, pH 7.5, 2 m*M* β-mercaptoethanol, and 2 m*M* $MgCl_2$ using a 1-mm quartz cuvette. Each far UV CD spectrum was obtained from an average of three scans and the results were presented as mean residue ellipticity (deg $cm^2$/dmol) at each wavelength. Near UV CD spectroscopy was carried out using 40 μ*M* of $EIC_{231–575}$ and 10 m*M* of substrates in 20 m*M* Tris-HCl, pH 7.4, 100 m*M* NaCl, 2 m*M* β-mercaptoethanol, and 4 m*M* $MgCl_2$ using a 10-mm quartz cuvette. Each near UV CD spectrum was obtained from an average of three scans and the results were presented as molar ellipticity (deg $cm^2$/dmol) at each wavelength.

### *Isothermal titration calorimetry of EIC with PEP and oxalate*

ITC experiments were performed at 25°C using an $ITC_{200}$ calorimeter (GE Healthcare). Twenty consecutive 2 μL aliquots of 3 m*M* PEP or 10 m*M* sodium oxalate were injected into the cell containing 0.25 or 0.5 m*M* $EIC_{231–575}$ in 20 m*M* Tris-HCl, pH 7.4, 100 m*M* NaCl, 2 m*M* β-mercaptoethanol, and 4 m*M* $MgCl_2$. The ITC experiments were also carried out in 20 m*M* sodium phosphate, pH 7.4, and 20 m*M* HEPES, pH 7.4, replacing the 20 m*M* Tris-HCl, pH 7.4 with the same buffer composition otherwise, to correct the binding heat by buffer contribution. The duration of each injection was 4 sec, and injections were made at intervals of 180 sec. Dilution heats of the substrates into the protein solution were subtracted from measured heats of the binding. ITC titration data were analyzed using the Origin software provided with the instrument.

## Acknowledgment

Authors thank the high field NMR facility at Korea Basic Science Institute for NMR experiments.

## References

1. Meadow ND, Fox DK, Roseman S (1990) The bacterial phosphoenolpyruvate glycose phosphotransferase system. Annu Rev Biochem 59:497–542.
2. Siebold C, Flükiger K, Beutler R, Erni B (2001) Carbohydrate transporters of the bacterial phosphoenolpyruvate: sugar phosphotransferase system (PTS). FEBS Lett 504:104–111.
3. Deutscher J, Francke C, Postma PW (2006) How phosphotransferase system-related protein phosphorylation regulates carbohydrate metabolism in bacteria. Microbiol Mol Biol Rev 70:939–1031.
4. Lee BR, Lecchi TS, Pannell L, Jaffe H, Peterkofsky A (1994) Identification of the N terminal domain of Enzyme I of the *Escherichia coli* phosphoenolpyruvate:-sugar phosphotransferase system produced by proteolytic digestion. Arch Biochem Biophys 3112:121–124.
5. Liao DI, Silverton E, Seok YJ, Lee BR, Peterkovsky A, Davies DR (1996) The first step in sugar transport: crystal structure of the amino terminal domain of Enzyme I of the *E. coli* PEP:sugar phosphotransferase system and a model of the phosphotransfer complex with HPr. Structure 4:861–872.
6. Garret DS, Seok YJ, Liao DI, Peterkovsky A, Gronenborn AM, Clore GM (1997) Solution structure of the 30 kDa N-terminal domain of Enzyme I of the *Escherichia coli* phosphoenolpyruvate:sugar phosphotransferase system by multidimensional NMR. Biochemistry 36: 2517–2530.
7. LiCalsi C, Crocenzi TS, Freire E, Roseman S (1991) Sugar transport by the bacterial phosphotransferase system: structural and thermodynamic domains of Enzyme I of *Salmonella typhimurium*. J Biol Chem 266:19519–19527.
8. Marquez JA, Reinelt S, Koch B, Engelmann R, Hengstenberg W, Scheffzek K (2006) Structure of the full-length Enzyme I of the phosphoenolpyruvate-dependent sugar phosphotransferase system. J Biol Chem 281:32508–32515.
9. Teplyakov A, Lim K, Zhu PP, Kapadia G, Chen CCH, Schwartz J, Howard A, Reddy PT, Peterkofsky A, Herzberg O (2006) Structure of phosphorylated Enzyme I, the phosphoenolpyruvate:sugar phosphotransferase system sugar translocation signal protein. Proc Natl Acad Sci USA 103:16218–16223.
10. Oberholzer AE, Schneider P, Siebold C, Baumann U, Erni B (2009) Crystal structure of Enzyme I of the phosphoenolpyruvate sugar phosphotransferase system in the dephosphorylated state. J Biol Chem 284: 33169–33176.
11. Oberholzer AE, Bumann M, Schneider P, Bachler C, Siebold C, Baumann U, Erni B (2005) Crystal structure of the phosphoenolpyruvate-binding Enzyme I-domain from the *Thermoanaerobacter tengcongensis* PEP:sugar phosphotransferase system (PTS). J Mol Biol 346: 5221–532.
12. Patel HV, Vyas KA, Mattoo RL, Southworth M, Perler FB, Comb D, Roseman S (2006) Properties of the C-terminal domain of Enzyme I of the *Escherichia coli* phosphotransferase system. J Biol Chem 281:17579–17587.
13. Brokx SJ, Talbot J, Georges F, Waygood EB (2000) Enzyme I of the phosphoenolpyruvate:sugar phosphotransferase system. In vitro intragenic complementation: the roles of Arg126 in phosphoryl transfer and the C-terminal domain in dimerization. Biochemistry 39: 3624–3635.
14. Suh JY, Cai M, Williams DC, Clore GM (2006) Solution structure of a post-transition state analog of the phosphotransfer reaction between the A and B cytoplasmic domains of the mannitol transporter $II^{Mannitol}$ of the *Escherichia coli* phosphotransferase system. J Biol Chem 281:8939–8949.
15. Suh JY, Iwahara J, Clore GM (2007) Intramolecular domain-domain association/dissociation and phosphoryl transfer in the mannitol transporter of *Escherichia coli* are not coupled. Proc Natl Acad Sci USA 104: 3153–3158.
16. Fomenkov A, Valiakhmetov A, Brand L, Roseman S (1998) In vivo and in vitro complementation of the N-terminal domain of Enzyme I of the *Escherichia coli* phosphotransferase system by the cloned C-terminal domain. Proc Natl Acad Sci USA 95:8491–8495.
17. Suh JY, Cai M, Clore GM (2008) Impact of phosphorylation on structure and thermodynamics of the interaction between the N-terminal domain of Enzyme I and the histidine phosphocarrier protein of the bacterial phosphotransferase system. J Biol Chem 283:18980–18989.
18. Garrett DS, Seok YJ, Peterkofsky A, Clore GM, Gronenborn AM (1998) Tautomeric state and pK, of the phosphorylated active site histidine in the N-terminal domain of Enzyme I of the *Escherichia coli* phosphoeno1pyruvate:sugar phosphotransferase system. Protein Sci 7:789–793.
19. Navdaeva V, Zurbriggen A, Waltersperger S, Schneider P, Oberholzer AE, Bahler P, Bachler C, Grieder A, Baumann U, Erni B (2011) Phosphoenolpyruvate:sugar phosphotransferase system from the hyperthermophilic *Thermoanaerobacter tengcongensis*. Biochemistry 50:1184–1193.
20. Misset O, Brouwer M, Robillard GT (1980) *Escherichia coli* phosphoenolpyruvate dependent phosphotransferase system. Evidence that the dimer is the active form of Enzyme I. Biochemistry 19:883–890.
21. Kukuruzinska MA, Turner BW, Ackers GK, Roseman S (1984) Subunit association of Enzyme I of the *Salmonella typhimurium* phosphoenolpyruvate:glycose phosphotransferase system. J Biol Chem 259:11679–11681.
22. Gomez J, Freire E (1995) Thermodynamic mapping of the inhibitor site of the aspartic protease endothiapepsin. J Mol Biol 252:337–350.
23. Goldberg RN, Kishore N, Lennen RM (2002) Thermodynamic quantities for the ionization reactions of buffers. J Phys Chem Ref Data 31:231–370.
24. Saier MH, Jr, Schmidt MR, Lin P (1980) Phosphoryl exchange reaction catalyzed by Enzyme I of the bacterial phosphoeno1pyruvate:sugar phosphotransferase system. J Biol Chem 255:8579–8584.
25. Dimitrova MN, Peterkofsky A, Ginsburg A (2003) Opposing effects of phosphoenolpyruvate and pyruvate with Mg2+ on the conformational stability and dimerization of phosphotransferase Enzyme I from *Escherichia coli*. Protein Sci 12:2047–2056.
26. Garcia-Alles LF, Alfonso I, Erni B (2003) Enzyme I of the phosphotransferase system: induced-fit protonation of the reaction transition state by Cys-502. Biochemisty 42:4744–4750.
27. Delaglio F, Grzesiek S, Vuister GW, Zhu G, Pfeifer J, Bax A (1995) NMRPipe: A multidimensional spectral processing system based on UNIX pipes. J Biomol NMR 6:277–293.
28. Johnson BA, Blevins RA (1994) NMRView: A computer program for the visualization and analysis of NMR data. J Biomol NMR 4:603–614.